

Up-scaling and stress dependency of permeability for soft fractured chalk

M. M. Lykke & N. Foged

Technical University of Denmark, Denmark

H. F. Christensen

GEO, Denmark

ABSTRACT: Fractures in reservoir chalk are a great benefit to production of oil, as the matrix permeability of oil bearing chalk reservoirs in the North Sea is low. It would be marginally economic to produce from many of these reservoirs without natural or induced fractures to enhance the effective permeability. To investigate the effect of fractures, absolute oil permeability tests on 5 large, fractured Hillerslev outcrop chalk specimens were performed in a centrifuge. The investigation also comprises permeability data on small, unfractured specimens and large, fractured specimens, extracted from earlier work on water-saturated Hillerslev outcrop chalk. The investigation includes correlation between fracture and matrix permeability, stress dependency and an evaluation on how to up-scale the laboratory observations to reservoir scale. Both permeability enhancement and reduction is seen as function of increased stresses. It is evaluated that the conventional centrifuge scaling for permeability and flow cannot be applied to fractured chalk.

1 INTRODUCTION

Oil displacement by waterflooding in fractured chalk is a very efficient recovery mechanism (Christensen 2003). To improve the modeling of chalk reservoirs and further increase the recovery, the displacement processes have to be understood especially in relation to the effect of fractures and stress dependency. More work is also required in relation to up-scaling of laboratory test results to reservoir scale.

Two earlier research projects, EFP-96, phase 1 (Havmøller et al. 1997) and EFP-98, phase 2 (Havmøller et al. 2001) present improved methods to predict rock mechanics properties in fractured reservoir zones. Methods for establishing an improved geological fracture model were developed and tested during phase 1. Phase 2 contained establishment of a fractured model integrating rock mechanics and geological descriptions, including up-scaling from laboratory to reservoir conditions. The aim was to investigate whether fracture effects could be related to strength and deformation properties and whether the effects could be up-scaled (Havmøller et al. 2001).

The EFP-98, phase 2 research project (Havmøller et al. 2001) comprises permeability data from tests on Hillerslev outcrop chalk. The permeability data were obtained mostly in connection with multiple triaxial and hydrostatic compaction tests. The tests were performed on two different sizes of specimens, i.e. diameter of 5.4 cm and 50 cm.

A continuation of this study was recently presented in a research project (Christensen 2003) carried out under the Danish Energy Research Programme 2000, EFP-2000. The work comprises quantification of displacement processes in fractured reservoir chalk. As part of the research project, an investigation of fractured chalk was carried out. The investigation was based on absolute oil permeability tests on large, fractured Hillerslev outcrop chalk specimens, modelled in a centrifuge. The modeling imply that at an acceleration of N times the gravitational acceleration, the test specimens can be considered to model the behavior of a reservoir volume of N times the dimensions of the specimen. The natural fractures in the test specimens may similarly represent a fractured reservoir.

In the present paper, the set-up, procedure and results for the absolute oil permeability tests are described. Further, a study of the correlation between fracture and matrix permeability and up-scaling of the laboratory observations to reservoir scale based on the test results are presented. Extracted permeability data from the EFP-98 project are used to facilitate the study of permeability stress dependency as most of these tests were carried out at higher mean stress levels than the EFP-2000 tests.

2 TEST MATERIAL

The Hillerslev outcrop chalk is of Late Maastrichtian age and highly fractured (Krogsbøll et al. 1997). Further, the chalk matrix is soft and homogeneous with a high porosity of approximately 47% and a very low clay content. The chalk is weakly cemented and can be described as autochthonous pelagic chalk (burrowed massive chalk mudstone). The effective depth of burial is > 300 m. The Hillerslev chalk was uplifted due to salt dome activity and the fracturing is assumed related to this uplift. The chalk is regarded as an analogue to a number of oil bearing chalk reservoirs in the North Sea, which have experienced similar salt movements.

2.1 Fracture descriptions

In order to investigate fracture flow, it is important to obtain knowledge of the fractures in the chalk. Both in connection with the centrifuge tests and earlier work on Hillerslev chalk, field trips were made to the Hillerslev outcrop chalk quarry located in the northern part of Jutland, Denmark. Here, a global fracture description was carried out and large ($D = 50$ cm and $H = 50$ cm) specimens were recovered.

A local fracture description was carried out for the test specimens and compared with the global fracture description (Lykke, 2003a). All the specimens were fractured to a higher or lesser degree, see figure 1. The most dominant fractures in the periphery of the specimens were very steeply dipping and seemed almost vertical. The local fracture description is in accordance with the global fracture observations, i.e. the fracture system in the specimens represents the major part of the Hillerslev outcrop chalk fracture pattern.



Figure 1. Photograph of the lower horizontal fracture plane in specimen 8 after test.

3 EXPERIMENTAL

Before test, the specimens were trimmed, measured, oven dried at 105° C and saturated with the light laboratory oil Isopar-L to a S_o of about 97-99 %. The density of the oil is $\rho = 0.763$ g/cm³ at 22° C and the dynamic viscosity is $\mu = 1.41$ cP at 22° C.

The test set-up, figure 2, includes a cylindrical form; an “oedometer cell” and two cylindrical endplates (top and bottom) to close the form. A porous filter ($D = 50$ cm) was fastened to the endplates. The specimen was placed on a porous filter on the bottom plate. A two-component rubber membrane was placed around the specimen to support and enclose it. The form was placed around the specimen, and the top plate with a porous filter was mounted. Two reservoirs was bolted onto the top plate, see figure 2. The inlet reservoir was used for oil flushing, and the outlet reservoir was used for displaced oil. The production to the outlet reservoir flowed through an overflow tube. To avoid flow along the side between the membrane and the specimen, a confining pressure was applied on the membrane through a tube on the form.

During testing, pore pressures were measured by pore pressure transducers (PPTs) to keep track of produced volumes and inlet and outlet pressures. PPT 5 was used to check the confining pressure to prevent side flow. PPT 1 and PPT 2 were used to keep track of produced volumes in the outlet reservoir. PPT 3 (overflow tube) measured the outlet pressure and PPT 4 measured the inlet pressure.

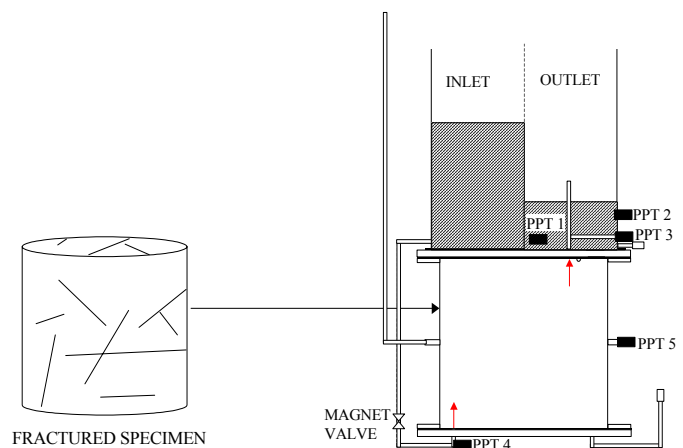


Figure 2. Specimen to be installed in the test set-up (PPT = pore pressure transducer).

After installation in the cylindrical form, the specimens were flushed with oil at 1 g via an approximately constant hydraulic pressure difference, to remove air entrapped during specimen handling after oil-saturation. The permeability was determined after the initial flushing.

The test set-up was installed in the centrifuge. The centrifuge rotor turns in a horizontal plane, with the model container and the counterweight hinged to

the rotor. The centrifuge was rotated resulting in application of 10, 20, 40 and 80 g at the specimen bottom. The radius to the specimen bottom is 2.565 m.

The centrifuge permeability tests were driven by a constant (specimen 7) or a falling hydraulic pressure difference resulting from the difference in inlet and outlet fluid heights. The centrifuge permeabilities were determined from the inflow and outflow pressures measured by the transducers, and the produced volumes of oil obtained from the transducers during the centrifuge tests.

The intrinsic permeability K [D] is determined by Darcy's law for slow, one-phase flow as (Dullien 1997):

$$K = \frac{Q \cdot \mu \cdot H}{A \cdot \Delta P} \quad (1)$$

where Q [cm^3/s] is the flow, μ [cP] is the dynamic fluid viscosity, H [cm] is the height of the specimen, A [cm^2] is the cross sectional area of the specimen and ΔP [atm] is the hydraulic pressure difference over the specimen. The Darcy flow domain is valid for Reynolds number, Re , lower than a limit value varying between 1 and 10, depending on materials and authors (Garnier et al. 2000). $Re = \rho \cdot v \cdot d / \mu$ where ρ [kg/m^3] is the fluid density, v [m/s] is the flow velocity, d [m] is a characteristic dimension of the flow here = the diameter of the specimen, and μ [Ns/m^2] is the dynamic fluid viscosity. The highest mean value of $Re = 13$ (peak $Re = 15.3$) was found for specimen 5 at 80 g, and at 40 g, mean $Re = 11$ and peak $Re = 13.7$. For the remaining permeabilities, both mean and peak values of Re are below 10. It is evaluated that the Darcy flow is valid for the tests.

4 RESULTS AND DISCUSSION

4.1 Fracture permeability data from centrifuge tests

The mean permeability is determined at each centrifuge step. The permeabilities are absolute, effective, oil permeabilities, given in table 1. The specimens are listed after degree of fracturing, based on inspection, with the most fractured specimen at the top.

Table 1. The absolute oil permeabilities at 1, 10, 20, 40 and 80 g for the 5 specimens.

Specimen	Permeability [mD]				
	1 g	10 g	20 g	40 g	80 g
2	206	351	623#	498	390
5	249	573	663	526	520
8	227	249	430	540	613
11	(31)*	18	18	18	19
7	8	9	7	7	(32)*

* Indication of side flow.

Permeability increase from 10 to 20 g without increase in hydraulic pressure difference.

The permeabilities obtained at 1 g for specimen 5, 8, 11 and 7 are in agreement with the degree of fracturing. Specimen 2 appears more fractured by inspection, but the fractures may not be as well connected since the 1 g permeability implies a lower degree of fracturing than specimen 5 and 8. The large increase from 1 to 10 g for specimen 5 may be caused by trapped air resulting in too low 1 g permeability.

In figure 3, permeability is plotted vs. the number of g (N) at the middle of the specimens, as N varies along the specimen. Permeability vs. mean stress is shown in figure 4. Only centrifuge permeability data is included. Further, the confining pressure was not measured at 10 g for specimen 2, and this step is thus not included.

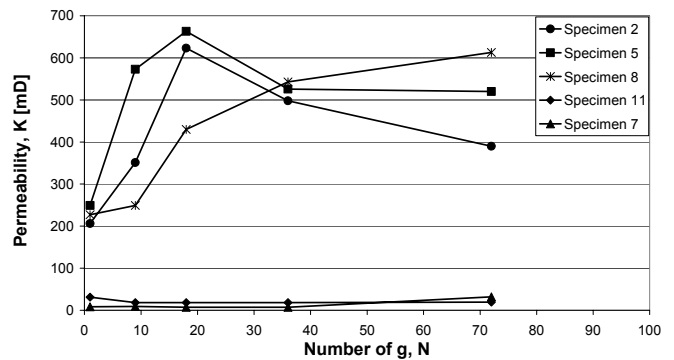


Figure 3. Permeability vs. number of g (N) calculated at the middle of the specimens, corresponding to application of 1, 10, 20, 40 and 80 g at the specimen bottom.

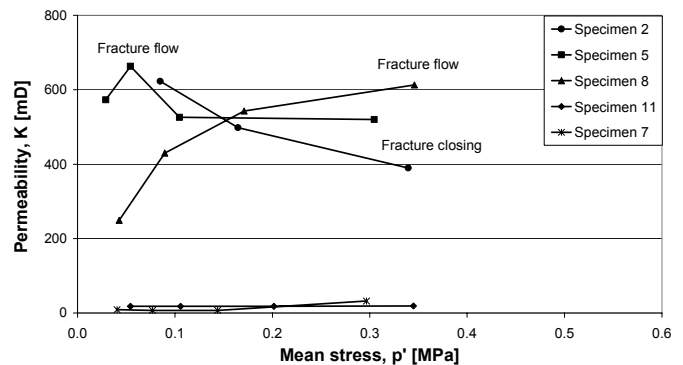


Figure 4. Mean stress vs. effective permeability at 10, 20, 40 and 80 g for specimen 2 (not at 10 g), 5, 8, 11 and 7.

The specimens clearly fall into two groups; specimen 2, 5 and 8 with high permeabilities in the range of 200-600 mD, and specimen 11 and 7 with low permeabilities in the range of 10-20 mD, see figure 3. The low permeabilities remain constant from 10 to 80 g, whereas increasing, constant and decreasing permeabilities are seen for the high permeabilities as the number of g increases. The permeabilities of the two most fractured specimens, 2 and 5, are closely following a similar trend, increasing from 1 to 20 g and then decreasing from 20 to 80 g. The permeability of the third most fractured specimen, 8, increases throughout the test. Until 40 g, the permeability of

specimen 8 is below the permeability of specimen 2 and 5. At 40 g, the permeability of the three specimens is approximately the same. From this centrifuge step on, the permeability “crosses over” and is higher for specimen 8 than for specimen 2 and 5. The permeability for the two least fractured specimens, 11 and 7, is approximately constant and low.

The three high permeability specimens also show a dependency on effective stress level, see figure 4. The permeability of specimen 2 and 5 is initially increasing with increasing stress level, below $p' \approx 0.1$ MPa, and then decreasing. The increase may be explained by fracture flow and rearrangement of fracture chalk pieces as the hydraulic pressure difference is also increasing except at 20 g. Specimen 2 and 5 show permeability decrease above a mean stress level of $p' \approx 0.1$ MPa, more pronounced in specimen 2 than in 5. Closing of some of the vertical fractures may explain the decrease. Note that after the fracture closing, the permeabilities are still very high. Both fracture flow and fracture closing may be explained by the “state” of the two specimens. Besides being the two most fractured specimens, specimen 5 contained crushed zones where the chalk was almost plastified, and zones with brittle chalk were seen in both specimens. Figure 5 shows an intense interconnected fracture pattern with plastified, crushed zones for specimen 5. The fluid flow might be influenced by some compaction and particle flow at higher stresses resulting in somewhat lower permeabilities.

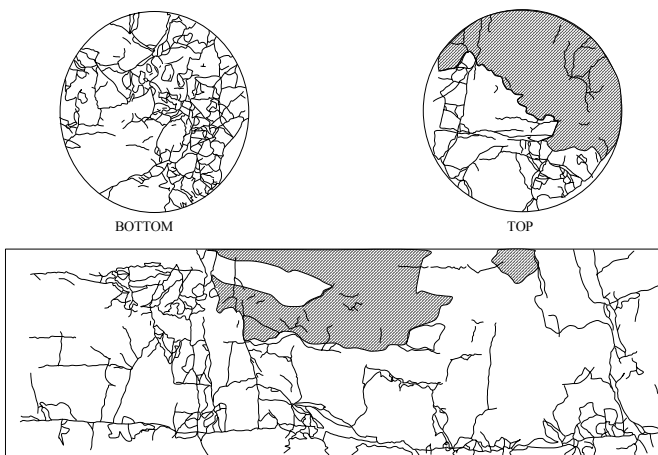


Figure 5. Fractures (black lines) at crushed zones (hatched) indicated on the top, bottom and periphery of specimen 5.

The permeability of specimen 8 is increasing throughout the test. As the hydraulic pressure difference is also increasing, there is indication of fracture flow. At the same time, the permeability may be influenced by possible closing of horizontal fracture planes due to application of vertical stresses. Specimen 8 has two continuing fracture planes, as indicated in figure 6, which may not be as “easy to close” as horizontal fractures.

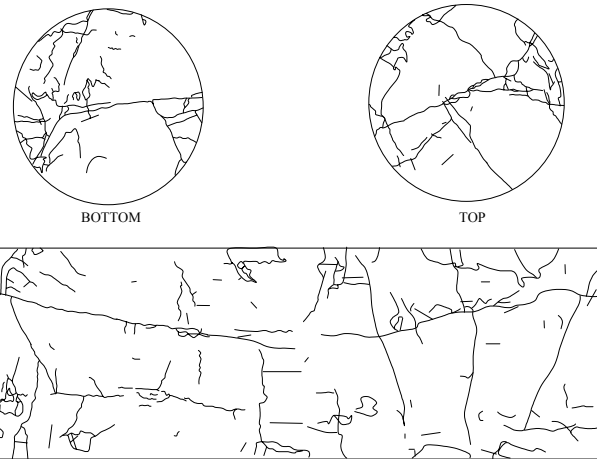


Figure 6. Fractures (black lines) indicated on the top, bottom and periphery of specimen 8.

Figure 6 shows a much “cleaner” fracture pattern for specimen 8, which is kept open during the entire test with increasing permeabilities.

4.2 Matrix permeability data

The EFP-98 project (Havmøller et al. 2001) includes permeability data from tests on small ($D = 5.4$ cm and $H/D \approx 2$), unfractured, water-saturated Hillerslev outcrop chalk specimens (HU 1, 2, 3 and 5). Multiple triaxial tests were carried out on HU 1, 2 and 3, and a hydrostatic compaction test was carried out on HU 5.

The matrix permeability can be compared to the small-scale tests carried out in the EFP-98 project with initial permeability in the range of $K = 2.1$ - 2.4 mD indicating homogeneous chalk. Indications of permeability decrease for increasing mean stress is observed from a single test loaded from 0.2 to 18 MPa with a corresponding permeability decrease from 2.5 to 0.3 mD.

The matrix permeability for small ($D \approx 3.8$ cm and $H \approx 5.0$ cm) unfractured Hillerslev outcrop chalk specimens in an earlier study was determined to 2.6-2.9 mD using synthetic Valhall formation water (Lykke 2003b).

4.3 Fracture permeability data from block specimens

The EFP-98 project (Havmøller et al. 2001) also includes permeability data from tests on large ($D = 50$ cm and $H/D \approx 1$), fractured, water-saturated Hillerslev outcrop chalk specimens (block 4, 6, 7, 8, 12, 13 and 15). Multiple triaxial tests were carried out on all the specimens.

The permeability is decreasing for increasing mean stress, figure 7. The most distinct permeability decreases are observed for block 8, 13 and 15.

Both the EFP-98 and the EFP-2000 large-scale tests show large initial permeabilities, reflecting that the fractures that opened during recovery in the field

and laboratory handling are not closed at the low initial stresses. The initial permeability drop at constant stress for block 13 and 15 may be explained by specimen disturbance.

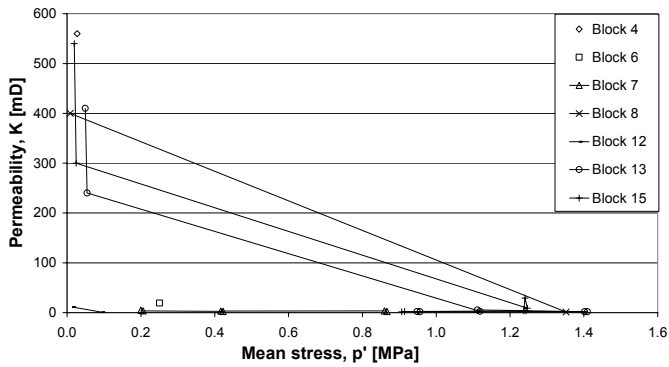


Figure 7. Mean stress vs. permeability for Hillerslev chalk based on the fractured EFP-98 block specimens.

Similarly as for the EFP-2000 specimens, the block specimens clearly fall into two groups; block specimen 4, 8, 13 and 15 with high permeabilities in the range of 200-600 mD, and block specimen 6, 7 and 12 with low permeabilities in the range of 1-20 mD. The low permeabilities remain constant for increase in stress level, but here the high permeabilities are decreasing to similar values as the low permeabilities as the stress level increases.

4.4 Stress dependency

To evaluate the stress states of the EFP-98 and EFP 2000 specimens, i.e. distinguish between elastic and plastic state, a shear failure criterion is necessary. In the EFP-98 project (Havmøller et al. 2001), the Hoek and Brown criterion (Hoek & Brown, 1997) was used to establish a shear failure model for Hillerslev outcrop chalk. The criterion calculates shear strength based on unconfined compressive strength for intact rock and “estimated” values of the Geological Strength Index, GSI (Hoek & Brown, 1997). The Hoek and Brown shear failure criterion for a jointed rock mass is:

$$\sigma_1' = \sigma_3' + \sigma_{ci} \cdot \left(m_b \cdot \frac{\sigma_3'}{\sigma_{ci}} + s \right)^a \quad (2)$$

where σ_1' is the maximum effective stress and σ_3' is the minimum effective stress. The rock mass constants; $m_b = m_i \cdot \exp((GSI-100)/28)$, $s = \exp((GSI-100)/9)$ and a is assumed to be $a = 0.5$ for $GSI > 25$. σ_{ci} is the unconfined compressive strength of intact rock. For intact rock mass, the shear failure criterion simplifies to:

$$\sigma_1' = \sigma_3' + \sigma_{ci} \cdot \left(m_i \cdot \frac{\sigma_3'}{\sigma_{ci}} + 1 \right)^{0.5} \quad (3)$$

where m_i is the rock mass constant for intact rock.

GSI provides overall values for fracture characterization of rock masses. $GSI = 100$ is assigned for intact chalk, i.e. for the small, unfractured specimens. GSI decreases as the specimens become more fractured, and $GSI = 65-75$ for the large, fractured block specimens before test.

The established failure model, see figure 8, is considered to be valid for the EFP-2000 specimens, as GSI values are comparable.

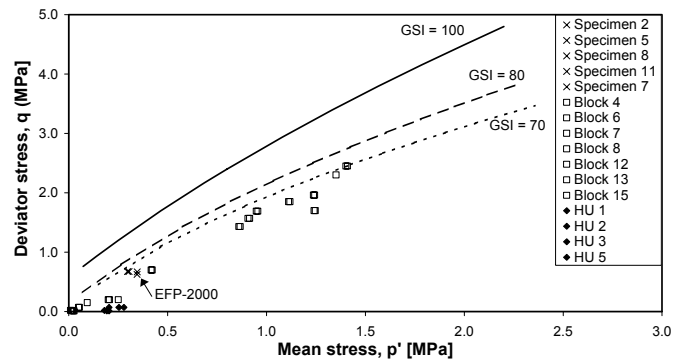


Figure 8. Hoek and Brown shear failure criteria for Hillerslev outcrop chalk. Data included for the unfractured EFP-98 specimens (HU), the fractured EFP-98 block specimens and the fractured EFP-2000 specimens at 80 g.

For the small-scale EFP-98 tests, the permeability measurements were carried out at low mean stress levels. However, the permeability reduction for the single small-scale test indicates stresses close to shear failure. High mean stress levels explain the permeability reduction for block 8, 13 and 15, indicating that these three specimens experienced stresses close to shear failure. For the EFP-2000 specimens, the stresses at 80 g are at significantly lower mean stress levels than block 8, 13 and 15. The specimens were not subjected to any vertical stress other than the self-weight.

4.5 Up-scaling

Laboratory measurements on small specimens cannot be applied directly to reservoir scale, as the effect of fractures has to be considered. Large, fractured specimens are considered more representative for reservoir scale, as the effect of more complex groups of natural fractures are included, see figure 9.

On the other hand, a small test plug recovered from a reservoir is representative for the place in question, but up-scaling of test results from this plug may not be representative for the entire reservoir.

5 CONCLUSIONS

A significant influence of fractures on permeability is seen. Presence of fractures increases the matrix permeability with a factor up to 200-300.

The results of the study show that the effect of the fractures is strongly connected to stress state. Higher stresses cause some closure of fractures with corresponding loss of permeability. Both permeability enhancement and reduction is seen as function of increased stresses, but the permeabilities are still high after reduction. A reason for permeability enhancement might be due to increasing fracture width due to rearrangement of fracture matrix chalk pieces.

Whether there is pronounced fracture flow is depending on the fracture system and whether the fractures are well connected or not. This is also affected by flow rate and fracture orientation.

The study also shows that when results are up-scaled, stress state has to be considered in connection with the fracture pattern.

Conventional centrifuge scaling for permeability (1:1) and flow (1:N) cannot be applied to fractured chalk.

Higher mean stress levels for the centrifuge tests are necessary to study permeability stress dependency.

6 ACKNOWLEDGEMENTS

The funding of this study by Danish Energy Authority, Mærsk Olie og Gas AS, Denmark and BP Norge, Norway is gratefully acknowledged.

7 REFERENCES

- Christensen, H. F. 2003. Displacement and deformation processes in fractured reservoir chalk. EFP-2000. GEO project no. 17787.
- Dullien, F. A. L. 1997. Porous media. Fluid transport and pore structure. 2. edition. Harcourt Publishers Ltd.
- Garnier, J., Thorel, L. & Haza, E. 2000. Proceedings of the int. symp. on Physical modelling and testing in environmental geotechnics.
- Havmøller, O. & Christensen, H. F. 1997. Fractures and rock mechanics. Phase 1. Geotechnical Report. EFP-96.
- Havmøller, O. & Krogsbøll, A. 2001. Fractures and rock mechanics. Phase 2.
- Hoek & Brown, E. T. 1997. Practical estimates of rock mass strength. Int. J. Rock Mech. Min. Sci. Vol. 34. No. 8. pp 1165-1186.
- Krogsbøll, A., Jakobsen, F. & Madsen, L. 1997. Fractures and rock mechanics. Phase 1. Geology Report. EFP-96.
- Lykke, M. M. 2003a. Hillerslev Outcrop Chalk. BYG DTU. Report no. R-20. ISSN 1601-2917, ISBN 87-7877-075-0. Technical University of Denmark.
- Lykke, M. M. 2003b. Capillary Pressure and Wettability Measurement on Hillerslev Outcrop Chalk. BYG DTU. Technical University of Denmark.

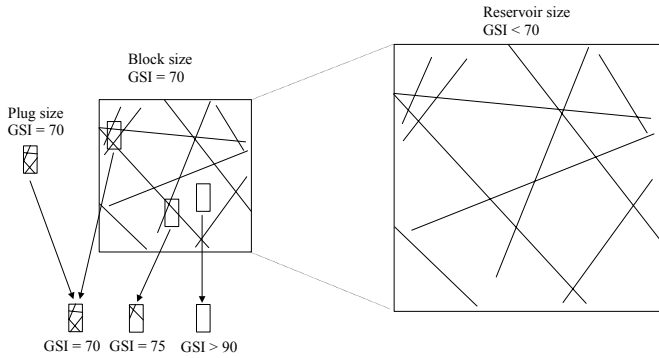


Figure 9. Up-scaling problems related to fracturing.

Conventional centrifuge up-scaling (Garnier et al. 2000) of permeability is 1:1, meaning that permeability is not scaled, and should be constant at each centrifuge step unless closing of fractures occurs.

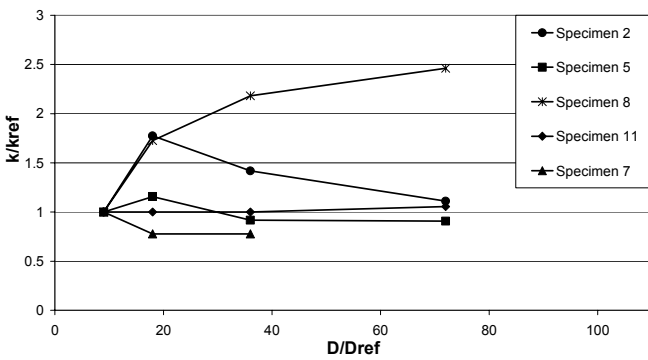


Figure 10. Permeability vs. diameter scaled in relation to 10 g.

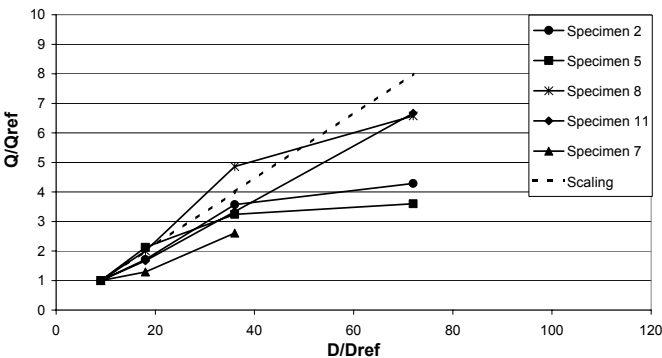


Figure 11. Flow vs. diameter scaled in relation to 10 g. The conventional scaling of flow is indicated by the dotted line.

However, as seen in figure 10, this is not the case for all the specimens. As discussed in the previous section, fracture closure is observed, especially in specimen 2 and 5. Specimen 8 shows fracture flow at high N and maximum stresses. Specimen 8 does not follow the conventional centrifuge scaling law for permeability. The least fractured specimens seem to follow the scaling law. For flow, conventional centrifuge upscaling (Garnier et al. 2000) is 1:N meaning that flow is up-scaled with N . None of the specimens seem to follow the conventional centrifuge scaling laws, see figure 11. Scaling is highly dependent on the reference value.